Translational Oncology
www.transonc.com

Volume 9 Number 5 October 2016 pp. 431–437 431

Noninvasive Assessment of Losartan-Induced Increase in Functional Microvasculature and Drug Delivery in Pancreatic Ductal Adenocarcinoma[1]

Vidhya Kumar*, Yves Boucher†, Hao Liu†, Diego Ferreira*, Jacob Hooker*, Ciprian Catana*, Andrew J. Hoover§, Tobias Ritter§,¶, Rakesh K. Jain† and Alexander R. Guimaraes*,‡

*Martinos Center for Biomedical Imaging, Department of Radiology, Massachusetts General Hospital, Charlestown, MA; †E.L. Steele Laboratories Department of Radiation Oncology Harvard Medical School and Massachusetts General Hospital 100 Blossom Street, Cox 7 Boston, MA 02114; ‡Division of Body Imaging, Department of Diagnostic Radiology, Oregon Health Sciences University, Portland, OR; §Department of Chemistry and Chemical Biology, Harvard University, 12 Oxford Street, Cambridge, Massachusetts 02138, United States; ¶Max-Planck-Institut fü r Kohlenforschung, Kaiser-Wilhelm-Platz 1, D-45470 Mü lheim an der Ruhr, Germany.

Abstract

PURPOSE: Losartan, an angiotensin II receptor blocker, can reduce desmoplasia and enhance drug delivery and efficacy through improving interstitial transport and vascular perfusion in pancreatic ductal adenocarcinoma (PDAC) models in mice. The purpose of this study was to determine whether magnetic resonance imaging (MRI) of magnetic iron oxide nanoparticles (MNPs) and micro–positron emission tomography (PET) measurements could respectively detect improvements in tumor vascular parameters and drug uptake in orthotopic PDAC in mice treated with losartan. *METHOD AND MATERIALS:* All experiments were approved by the local Institutional Animal Care and Use Committee. FVB mice with orthotopic PDAC were treated daily with an i.p. injection of losartan (70 mg/kg) or saline (control vehicle) for 5 days. In order to calculate the fractional blood volume, vessel size index, and vessel density index, MRI was performed at 4.7 T following the injection of 3 mg/kg iron ferumoxytol (i.v.). Dynamic PET images were also acquired for 60 minutes using an ^{18}F-5FU tracer dose of 200 μCi and analyzed for time activity curves normalized to muscle. Statistical analyses compared both cohorts using an unpaired two-tailed *t* test. RESULTS: In comparison to the control treatment, the losartan administration significantly increased the fractional blood volume (mean ± SEM) [12.1 ± 1.7 (n = 19) vs 6.7 ± 1.1 (n = 20); P < .02] and vessel size index (128.2 ± 35.6 vs 57.5 ± 18; P < .05). Losartan also induced a significant increase in the intratumoral uptake of ^{18}F-5FU by 53% (P < .0001). *CONCLUSION:* MRI using FDA-approved MNPs provides a noninvasive, translatable means of assaying microvascular parameters induced by losartan in pancreatic cancer. PET measurements demonstrated that losartan significantly increased the uptake of ^{18}F-5FU.

Translational Oncology (2016) 9, 431–437

Address all correspondence to: Alexander R. Guimaraes, MD, PhD, Associate Professor of Radiology, Section Chief, Body Imaging, Department of Diagnostic Radiology, Oregon Health Sciences University, 3181 SW Sam Jackson Park Road, Mail Code L340, Office SJH 10B77, Portland, OR, 97239, or Yves Boucher, PhD, Steele Lab for Tumor Biology, Department of Radiation Oncology, Massachusetts General Hospital, 149 13th St., Charlestown, MA, 02129. E-mail: guimaraa@ohsu.edu

[1] Funding: A. R. G. acknowledges the National Institutes of Health grant K08 EB 012859-04, and Y. B. and R. K. J. acknowledge the National Institutes of Health grants P01-CA080124 (R. K. J.), R01-CA098706 (Y. B.), and R21CA173518 (Y. B.) and a grant from the Lustgarten Foundation.
Received 27 May 2016; Accepted 18 July 2016

1936-5233/16
http://dx.doi.org/10.1016/j.tranon.2016.07.004

Introduction

Pancreatic ductal adenocarcinoma (PDAC) is a devastating illness that responds poorly to chemotherapy. The poor survival of patients with unresectable PDAC is partly due to the fact that extant chemotherapeutic options have dismal efficacy in humans [1,2]. In PDAC, the desmoplastic reaction rich in extracellular matrix constituents like collagen fibers and hyaluronan is a significant barrier, which limits the therapeutic efficacy of cytotoxic agents [3–5]. The solid pressure/stress produced by the dynamic interaction between cancer cells, stromal cells, and the extracellular matrix compresses blood vessels, which reduces the tumor blood flow and

drug delivery [3,6–8]. In PDAC models, stromal modifiers, which reduce desmoplasia, can improve vascular perfusion, drug delivery, and the effectiveness of cytotoxic agents [3–5,9]. In a transgenic mice model of PDAC, PEGPH20, a recombinant enzyme which degrades hyaluronan, reduced the hyaluronan content and enhanced vascular perfusion and the efficacy of gemcitabine [5]. We have shown that the angiotensin II receptor blocker losartan—which inhibits the activity of TGF-β and other profibrotic cytokines—reduces the levels of collagen and hyaluronan in orthotopic PDAC models [3,10]. Furthermore, losartan increased the fraction of perfused vessels and the delivery and efficacy of 5-fluorouracil (5FU) [3]. Losartan also increased the efficacy of the nanotherapeutic Doxil [10]. Interestingly, the administration of 5FU, Doxil, or losartan alone did not affect the growth of pancreatic tumors, but tumors were significantly smaller in mice treated with losartan combined with either Doxil or 5FU [3,10]. Thus, losartan shows potential as an adjunct to safely enhance the intratumoral penetration and efficacy of small and large therapeutics in patients with pancreatic cancer. Losartan combined with the folinic acid (leucovorin), fluorouracil (5-FU), irinotecan (Camptosar), oxaliplatin (Eloxatin) (FOLFIRINOX) cocktail is now being evaluated in patients with locally advanced unresectable pancreatic cancer (NCT01821729).

An unmet need in clinical imaging is a noninvasive, translatable approach to measure microvascular changes in humans. The malignant neovasculature has been shown to be hyperpermeable to molecules [11–22]. Due to this hyperpermeability, Dynamic contrast-enhanced magnetic resonance imaging (MRI) with Gadolinium - diethylenetriaminepentaacetic acid (Gd-DTPA) provides a noninvasive, quantitative measure (e.g., K_{trans}) of response to novel antiangiogenic drugs in hypervascular malignancies [11–22]. Blood vessel density, however, is known to be markedly lower in PDAC [4], which may explain its poor response to antiangiogenic therapies and which makes PDAC a poor choice for interrogation with dynamic techniques. Because of its long intravascular blood pool resident time, MRI with magnetic nanoparticles (MNPs) is a better imaging method for PDAC because it offers a steady-state solution for precise measurements of microvascular parameters [23–26]. Steady-state techniques are also ideally suited to study PDAC in humans because respiratory motion and luminal gas surrounding the pancreas severely limit dynamic techniques. We and others have shown in xenograft models implanted subcutaneously that MRI of MNPs provides a noninvasive, accurate assessment of fractional blood volume (fBV) and vessel size index (VSI) [24–34].

The poor efficacy of chemotherapy in PDAC concomitant with the exciting potential of increased drug uptake induced by angiotensin II receptor blocker (ARB) in a PDAC model represents a challenge for noninvasive imaging methods assessing tumor vascular parameters and drug delivery in preclinical and human tumors. The goal of this study was to determine whether MRI with MNPs is a valid noninvasive, steady-state surrogate biomarker of the functional neovasculature in an orthotopic mouse model of PDAC. We determined the relationship of the steady-state shifts ΔR2 and ΔR2* in the transverse relaxation rates 1/T2 and 1/T2* caused by injection of long circulating MNPs by modeling the fBV (~ΔR2*), VSI (~$\Delta R2^*/\Delta R2)^n$, and vessel density index (VDI) [$\Delta R2/(\Delta R2^*)^n$] [24–34]. Given the low vascular density in PDAC, morphologic indices such as fBV, VSI, and VDI may be more insightful measures of indirect effects on the tumor vasculature than measurements derived from dynamic approaches (e.g., K_{trans}). We also hypothesize that MRI will be sensitive to losartan-induced changes in the PDAC vasculature. Furthermore, we hypothesize that changes in the PDAC vasculature are linked to changes in drug delivery as determined by micro–positron emission tomography (PET) measurements of ^{18}F-5FU uptake.

Materials and Methods

Drug Preparation

Losartan pills (50 mg/pill) (Merck Pharmaceuticals, Inc.. Kenilworth, NJ)—obtained from the Massachusetts General Hospital pharmacy—were crushed and dissolved in PBS over 24 hours as previously described [3,10]. The solutions were then sterile filtered for injection.

Animal Model and Tumor Treatment Protocol

All experiments were approved by the Massachusetts General Hospital Institutional Animal Care and Use Committee. AK4.4 cells were originally isolated from the PDAC lesions of a genetically engineered mouse model (Ptfl-Cre/LSL-KrasG12D/p53Lox) [35]. Orthotopic tumors were generated by implanting 1-mm^3 chunks of AK4.4 in the pancreas of 6- to 8-week-old FVB mice. Mice with AK4.4 tumors were separated into two groups (losartan and control). Animals were treated daily with an intraperitoneal (i.p.) injection of losartan (70 mg/kg) or saline (control) for 5 days. Animals were sacrificed after a 5-day course of treatment and imaging.

Magnetic Resonance Imaging

MRI was performed at 4.7 T on a Bruker imaging system (Biospin, Karlsruhe, Germany). Animals were imaged after 5 days of therapy. Animals were anesthetized during imaging with 1% to 1.5% inhaled isoflurane and monitored during imaging with respiratory monitoring. Imaging protocols included a Tri-plane and axial RARE localizer. Multislice multiecho T2-weighted imaging was performed prior to and following intravenous injection of MNPs (10 mg/kg Fe, ferumoxytol, Feraheme; AMAG Pharma, Waltham, MA). The following parameters were utilized: Multiecho spin echo T2 maps were acquired with the following parameters: flip angle =90°; matrix size = 128 × 64; repetition time (TR) = 2000 milliseconds; echo time (TE) = 6 equally spaced echoes at 10-millisecond intervals ranging from 10 to 60 milliseconds; field of view (FOV) = 4.24 × 2.12 cm; slice thickness = 1 mm. Multiecho gradient echo T2* maps were acquired with the following parameters: flip angle =60°; matrix size = 128 × 128; TR = 750 milliseconds; TE = 4 equally space echvoes at 5 msec; FOV = 4.24 × 2.12 cm; slice thickness = 1 mm. T1-weighted imaging was performed following the administration of intravenous Gd-DTPA utilizing the following parameters: flip angle =90°; matrix size = 256 × 256; TR = 700 milliseconds; TE =14 milliseconds; FOV = 4.24 × 2.12 cm; slice thickness = 1 mm.

MRI Data Analysis

All data were analyzed in Matlab using code written in-house. fBV, VSI, and VDI values were obtained by defining a region of interest (ROI) over the entire tumor area. This process was repeated for three central slices of the tumor for every animal, and the mean value within the ROI was calculated. T2 and T2* values were obtained using gradient echo (GRE) and spin echo (SE) data, respectively, by plotting mean ROI value at each echo and calculating the best-fit exponential decay function. R2 and R2* were defined as the inverse of T2 or T2* values; ΔR^*_2 and ΔR_2 were calculated as the ratio of values before and after iron contrast injection.

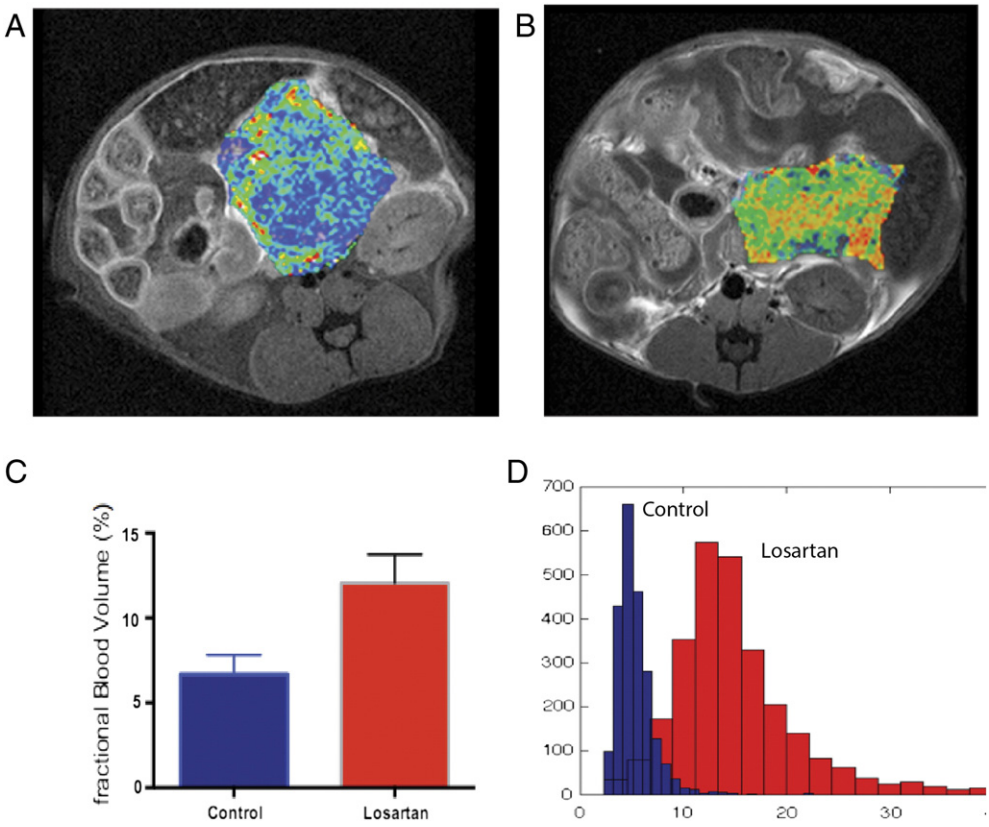

Figure 1. T1-weighted axial MR images of mice status postimplantation of AK4.4 orthotopically in the tail of the pancreas, with pseudocolorized maps of fBV (A, B) overlying the tumors. These maps were obtained after injection of the ferumoxytol, the FDA-approved nanoparticle. Note the increased distribution of fBV in the losartan-treated animals (B) as compared to controls (A). Histogram analysis demonstrates a right shift in pixels as obtained from ROI analysis within the central slice of the losartan-treated animals in fBV (D). ROI analysis of the three central slices was performed in all animals. The bar graphs demonstrate a nearly two-fold increase in fBV (C) ($P < .02$) in losartan-treated animals ($n = 19$) (mean ± SEM) (12.1 ± 1.7) compared to the control group ($n = 20$) (6.7 ± 1.1) ($P < .02$).

fBV of the tumor was derived from the relationship of ΔR^*_2, fBV, and magnetic field constants (γ, B_0) to changes in magnetic susceptibility, $\Delta\chi$.

$$\Delta\chi = \frac{3}{4\pi}\frac{\Delta R^*_{2,\text{muscle}}}{\text{fBV}_{\text{muscle}}\gamma B_0} = \frac{3}{4\pi}\frac{R^*_{2,\text{tumor}}}{\text{fBV}_{\text{tumor}}B_0}$$

$$\frac{3}{4\pi}\frac{R^*_{2,\text{muscle}}}{\text{fBV}_{\text{muscle}}\gamma B_0} = \frac{3}{4\pi}\frac{\Delta R^*_{2,\text{tumor}}}{\text{fBV}_{\text{tumor}}B_0}$$

$$\text{fBV}_{\text{tumor}} = \text{fBV}_{\text{muscle}}\frac{\Delta R^*_{2,\text{tumor}}}{\Delta \text{R}^*_{2,\text{muscle}}}$$

where $\text{fBV}_{\text{muscle}}$ is assumed to be a constant of 3%.

VSI was computed using the following equation:

$$\text{VSI} = 0.424\left(\frac{\text{ADC}}{\gamma\Delta\chi\text{B}_0}\right)^{1/2}\frac{\Delta R^*_2}{\Delta R_2}$$

For normalized value calculations, the first two terms were considered to be constant for all images and were therefore disregarded.

VDI was computed as follows:

$$\text{VDI} = 329\frac{\Delta R_2}{\Delta R^*_2}$$

As for the VSI calculations, the first term in the VDI equation was disregarded during calculation of normalized values [33].

Paramagnetic maps were generated by calculating VSI, VDI, and fBV values on a voxel-by-voxel basis. Histograms were obtained by plotting vessel indices within a tumor ROI against the frequency of occurrence.

Data are reported as fBV, VSI, and VDI ± standard error of the mean.

Positron Emission Tomography

MicroPET studies were performed on a Triumph PET/CT Scanner (GE Medical Systems, Waukena, WI). A separate trial was performed using the identical animal model and treatment protocol in order to assess whether losartan demonstrated increased drug delivery as measured by ^{18}F-5FU using dynamic imaging over 1 hour. These experiments were performed on separate days and used control and treated pairs in order to minimize scanner and radioisotope production bias. $N = 5$ pairs of orthotopic pancreatic tumor model mice were anesthetized using isoflurane and imaged in treated-control pairs. Dynamic PET images were acquired for 60 minutes using an ^{18}F-5FU tracer dose of 200 μCi per animal. Computed tomographic (CT) scans for attenuation and anatomic co-registration were performed immediately following PET acquisition. ROI analysis was performed on dynamic co-registered images using Osirix with time activity curves normalized to muscle. Initial area under the curve was performed on normalized curves and then compared to controls.

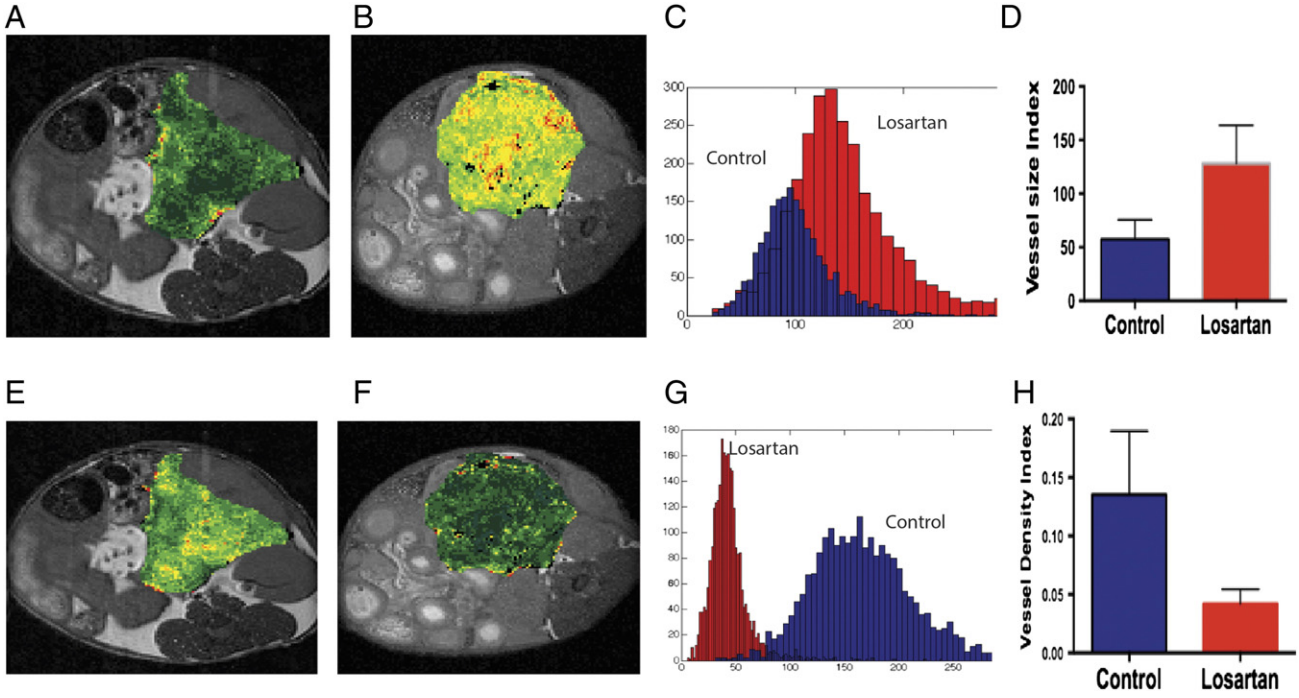

Figure 2. T1-weighted axial MR images of mice status postimplantation of AK4.4 orthotopically in the tail of the pancreas, with pseudocolorized maps of fractional blood volume (VSI) (A, B), and VDI (E, F) overlying the tumors. These maps were obtained after injection of the ferumoxytol, the FDA-approved nanoparticle. Note the increased distribution of VSI in the losartan-treated animals (B) as compared to controls (A). In addition, note the decrease in VDI in the losartan-treated animal (D) as compared to the control (C). Histogram analysis demonstrates a right shift in pixels as obtained from ROI analysis within the central slice of the losartan-treated animals in VSI (D) and a left shift of pixels in VDI (F). Histogram analysis (C) demonstrates a shift in VSI in losartan-treated animals as compared to control, and ROI analysis of the central three slices demonstrated a significant increase in VSI (128.2 ± 35.6 vs 57.5 ± 18) ($P < .05$) in losartan than control animals.

Statistical Analysis

Statistical analyses of MRI data compared both cohorts losartan ($n = 19$) and control ($n = 20$) using an unpaired two-tailed t test of unequal variances. Analysis of PET data ($n = 5$ pairs) were performed using a two-tailed paired t test of unequal variances.

Results

Magnetic resonance imaging (MRI)

Figure 1 demonstrates pseudocolorized fBV (*A* and *B*) superimposed over T1-weighted postcontrast images at the middle level of orthotopic tumors, in the region near the tail of the pancreas. Note the heterogeneous increase in fBV in the losartan-treated cohort (Figure 1*B*) in comparison to the saline-treated cohort (Figure 1*A*). ROI analysis of the three central slices of each tumor demonstrated a nearly two-fold significant increase in fBV ($P < .02$) in losartan-treated cohort (mean ± SEM) (12.1 ± 1.7, $n = 19$) compared to control (6.7 ± 1.1, $n = 20$) (Figure 1*C*). This is corroborated by histogram analysis (Figure 1*D*) of the fBV data demonstrating a shift to the right in the losartan-treated cohort compared to control.

Similarly, we found a heterogeneous increase in VSI in losartan-treated compared to control mice (Figure 2, *A* and *B*). Histogram analysis (Figure 2*C*) demonstrates a shift in VSI in losartan-treated animals as compared to control, and ROI analysis of the central three slices demonstrated a significant increase ($P < .05$) in VSI (128.2 ± 35.6 vs 57.5 ± 18) in losartan versus control animals.

Paradoxically, there was an increase in VDI visually in the pseudocolorized VDI map in the control-treated (Figure 2*E*) cohort as compared to the losartan-treated cohort (Figure 2*F*), most notable in the periphery than the tumor center. This was also replicated in the histogram analysis (Figure 2*G*), and when performing the quantitative ROI analysis, the VDI was significantly higher ($P < .05$) in control- (0.15 ± 0.06) than losartan- (0.04 ± 0.01) treated animals.

Losartan Increases Drug Delivery in Orthotopic PDAC

^{18}F-5FU microPET was performed in losartan-treated mice and paired control mice ($n = 5$ pairs) in order to minimize and remove bias from radioisotope production and attenuation correction. Figure 3 demonstrates attenuated corrected microPET images in control- (Figure 3*A*) and losartan-treated (Figure 3*B*) tumors 60 minutes after the injection of ^{18}F-5FU. Figure 3*C* is a representative T1-weighted postcontrast image with a large, enhancing tumor anterior to the left kidney. ROI analysis of fused CT images was performed on kinetic data acquired at the midpoint of the tumor, liver, muscle, kidney, and spleen. Kinetic curves are shown for the tumor in the losartan-treated (red) versus control-treated (blue) animals. The area under the curve analysis demonstrated a significant increase (~53%) in 5FU delivery within the tumor of losartan-treated animals ($P < .001$, Figure 3*E*). Losartan did not affect the uptake of ^{18}F-5FU in the liver (Figure 3*F*), kidney, muscle, or spleen.

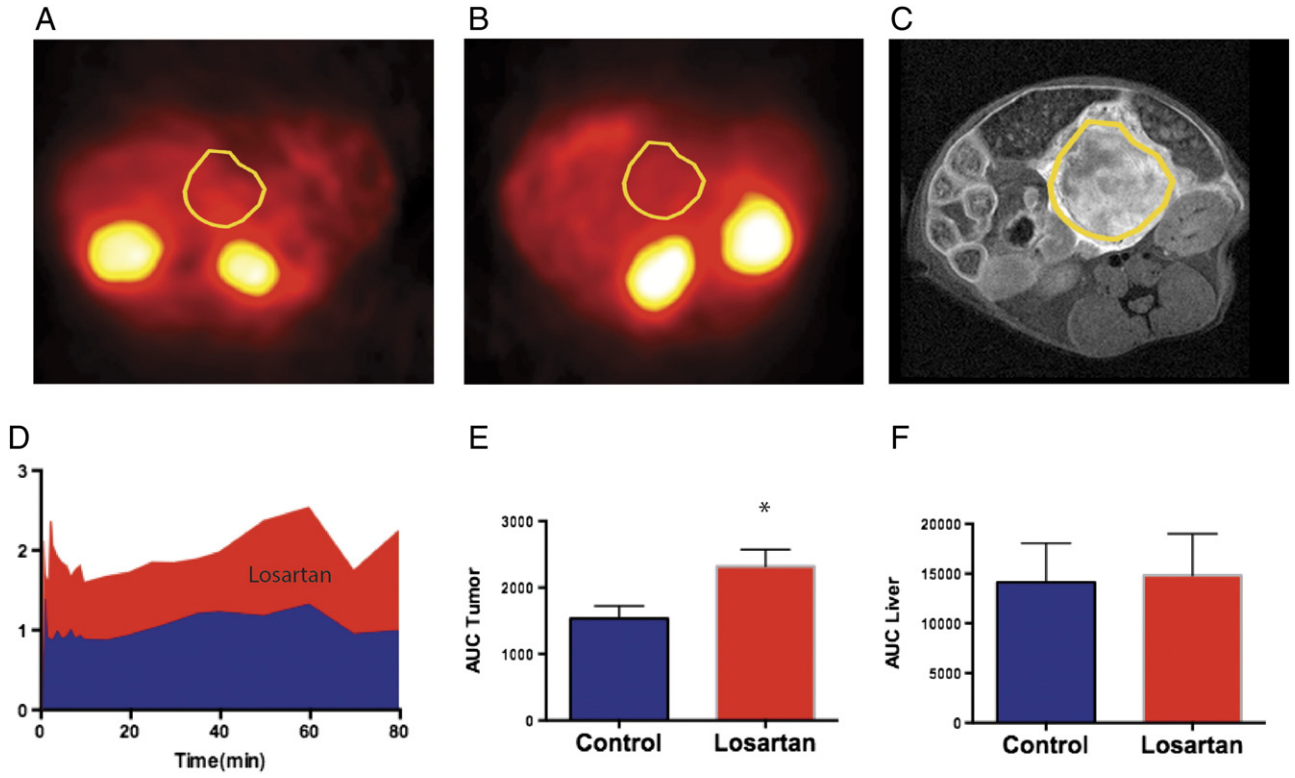

Figure 3. MicroPET images after injection of 200 μCi of 18F-5FU of two mice status post orthotopic implantation of PDAC anterior to the left kidney [(A) control and (B) losartan] treated for 5 days i.p. ROIs are overlying the tumor from CT images.(C) A representative example of the tumor is shown from a T1-weighted image at 4.7 T status post i.v. injection of Gd-DTPA. (D) Average (n = 5) time activity curves for uptake from an ROI overlying the entirety of the tumor normalized to muscle activity. Note the ~50% increase (red area under the curve) in activity in the losartan-treated cohort as compared to the control-treated cohort (blue). (E) Area under the curve analysis of tumor activity normalized to muscle activity in n = 5 animals. Statistical analysis of the studies using a paired t test (P .001) demonstrates an approximately 53% increase in drug delivery in the losartan-treated animal cohorts compared to control.

Discussion

MRI provides high–spatial resolution, noninvasive imaging of anatomy with high soft tissue contrast. Dynamic contrast-enhanced MRI techniques with the small molecule gadolinium-based contrast agents are sensitive to changes in the tumor microvasculature but have limited applicability in the human pancreas because of motion and overlying gas [24–34]. Steady-state techniques using magnetic nanoparticles provide a noninvasive, accurate, and sensitive assessment of fBV, which was considered a surrogate marker of microvessel density in subcutaneous pancreatic tumor xenografts [23–26]. This study expands on these previous studies and shows that MRI of MNPs is a noninvasive and valid approach to quantify microvascular parameters in orthotopic PDAC lesions.

Our findings demonstrate that MR measurements of MNPs can measure changes in fBV, VSI, and VDI induced by the ARB losartan [26,30,32,34]. Losartan significantly increased the fBV and VSI by approximately two-fold. In the same orthotopic AK4.4 PDAC model—based on measurements in histological sections—we found that losartan significantly increased the fractions of both perfused vessel and vessels with an open lumen [3,10]. The increased fBV induced by losartan could result from the increased fraction of perfused vessels and vessels with larger lumens. The lack of measurement of the apparent diffusion coefficient limits the accuracy of VSI measurements [32,34]. However, as mentioned above, losartan significantly increased the fraction of vessels with an open lumen [3], which supports our MRI estimates of VSI that also increased following losartan. The significant decrease in VDI could be due to the higher dose of losartan (70 mg/kg) in comparison to the lower dose of losartan (40 mg/kg) in our previous study [3]. In other studies, the genetic deletion of AT1R and high doses of ARBs or losartan significantly reduced the tumor microvessel density [36,37]. Thus, MR measurements of FDA-approved magnetic nanoparticles represent a valid approach to interrogate noninvasively the pancreatic tumor microvasculature in pancreatic cancer patients.

Our microPET measurements demonstrate that, in comparison to the control group, losartan significantly increased the intratumoral uptake of ^{18}F-5FU by 53%, which is comparable to the 74% increase in 5FU uptake measured by reverse-phase high-performance liquid chromatography with tandem mass spectrometry in orthotopic AK4.4 tumors [3]. Furthermore, similar to our previous findings [3], losartan did not affect the uptake of ^{18}F-5FU in the liver, kidney, muscle, or spleen. Given the improved efficacy of the FOLFIRINOX cocktail—which includes the drug 5FU—in patients with pancreatic cancer and our results demonstrating improved drug delivery with two different methodologies, at different scales, the translatable aspect of microPET ^{18}F-5FU measurements is important.

There are potential shortcomings with *in vivo* drug uptake measurements based on ^{18}F-5FU. 5FU rapidly metabolizes in plasma, and therefore, since it could not be assayed, it is unclear which metabolite of 5FU was measured by microPET in tumors.

Because both losartan and control mice were treated and imaged in pairs and ARBs are not known to increase the metabolism of 5FU, it is assumed that the metabolism was equivalent in both losartan and control mice.

In summary, we demonstrate that MRI and microPET can measure changes in vascular parameters and drug uptake induced by losartan in a pancreatic cancer model. Our MRI findings support the hypothesis that ARBs increase the functional microvasculature and, more importantly, that MRI of magnetic nanoparticles is sensitive to these changes. Because microPET and high-performance liquid chromatography measured comparable values of drug uptake, microPET and MRI represent *in vivo* approaches that can measure the changes in the PDAC microenvironment produced by stromal modifiers. Furthermore, our findings suggest that MRI and microPET measurements can be readily translated to patients with pancreatic cancer.

Paradoxically, there was an increase in VDI visually in the pseudocolorized VDI map in the control-treated (E) cohort as compared to the losartan-treated cohort (F), most notable in the periphery as compared to the central tumor. This was also replicated in the histogram analysis (G), and when performing quantitative ROI analysis, the losartan-treated animals (0.04 ± 0.01) were lower in VDI as compared to the control animals (0.15 ± 0.06) ($P < .05$).

Translational Relevance: In pancreatic ductal adenocarcinoma (PDAC), the interaction between the desmoplastic stroma and cancer cells generates physical forces that compress microvessels, thus reducing vascular perfusion and the delivery of therapeutics. We have shown that the angiotensin II receptor blocker losartan reduces desmoplasia and improves vascular perfusion and drug uptake in PDAC models. Magnetic resonance imaging (MRI) using FDA-approved magnetic nanoparticles and positron emission tomography (PET) are robust steady-state technique that, unlike intravital microscopy or histologic measurements, are readily translatable to humans and scalable from mice to humans. The aim of this study was to refine and apply MRI- and microPET-based methods to noninvasively measure changes in microvascular parameters and drug uptake (18F-5-fluorouracil) in a murine model of PDAC in response to losartan. We show here that MRI and microPET approaches detect increases in microvascular parameters and drug uptake induced by losartan. Our results suggest that MRI and microPET techniques are readily translatable to human and could be used to determine the effects of stromal modifiers in the lesions of pancreatic cancer patients.

Acknowledgements

Conflict of interest: R. K. J. owns equity in Enlight, Ophthotech, SynDevRx, and XTuit and serves on the Board of Directors of XTuit and the Boards of Trustees of Tekla Healthcare Investors, Tekla Life Sciences Investors, the Tekla Healthcare Opportunities Fund, and the Tekla World Healthcare Fund. No agent or funding from any of these organizations was used in this study.

References

[1] Hidalgo M and Von Hoff DD (2012). Translational therapeutic opportunities in ductal adenocarcinoma of the pancreas. *Clin Cancer Res* **18**, 4249–4256.

[2] Ryan DP, Hong TS, and Bardeesy N (2014). Pancreatic adenocarcinoma. *N Engl J Med* **371**, 2140–2141.

[3] Chauhan VP, Martin JD, Liu H, Lacorre DA, Jain SR, Kozin SV, Stylianopoulos T, Mousa AS, Han X, and Adstamongkonkul P, et al (2013). Angiotensin inhibition enhances drug delivery and potentiates chemotherapy by decompressing tumour blood vessels. *Nat Commun* **4**, 2516–2527.

[4] Olive KP, Jacobetz MA, Davidson CJ, Gopinathan A, McIntyre D, Honess D, Madhu B, Goldgraben MA, Caldwell ME, and Allard D, et al (2009). Inhibition of Hedgehog signaling enhances delivery of chemotherapy in a mouse model of pancreatic cancer. *Science* **324**, 1457–1461.

[5] Provenzano PP, Cuevas C, Chang AE, Goel VK, Von Hoff DD, and Hingorani SR (2012). Enzymatic targeting of the stroma ablates physical barriers to treatment of pancreatic ductal adenocarcinoma. *Cancer Cell* **21**, 418–429.

[6] Boucher Y and Jain RK (1992). Microvascular pressure is the principal driving force for interstitial hypertension in solid tumors: implications for vascular collapse. *Cancer Res* **52**, 5110–5114.

[7] Padera TP, Stoll BR, Tooredman JB, Capen D, di Tomaso E, and Jain RK (2004). Pathology: cancer cells compress intratumour vessels. *Nature* **427**, 695–699.

[8] Stylianopoulos T, Martin JD, Chauhan VP, Jain SR, Diop-Frimpong B, Bardeesy N, Smith BL, Ferrone CR, Hornicek FJ, and Boucher Y, et al (2012). Causes, consequences, and remedies for growth-induced solid stress in murine and human tumors. *Proc Natl Acad Sci U S A* **109**, 15101–15108.

[9] Long KB, Gladney WL, Tooker GM, Graham K, Fraietta JA, and Beatty GL (2016). IFNgamma and CCL2 Cooperate to Redirect Tumor-Infiltrating Monocytes to Degrade Fibrosis and Enhance Chemotherapy Efficacy in Pancreatic Carcinoma. *Cancer Discov* **6**, 400–413.

[10] Diop-Frimpong B, Chauhan VP, Krane S, Boucher Y, and Jain RK (2011). Losartan inhibits collagen I synthesis and improves the distribution and efficacy of nanotherapeutics in tumors. *Proc Natl Acad Sci U S A* **108**, 2909–2914.

[11] Barrett T, Brechbiel M, Bernardo M, and Choyke PL (2007). MRI of tumor angiogenesis. *J Magn Reson Imaging* **26**, 235–249.

[12] Coenegrachts K, Van Steenbergen W, De Keyzer F, Vanbeckevoort D, Bielen D, Chen F, Dockx S, Maes F, and Bosmans H (2004). Dynamic contrast-enhanced MRI of the pancreas: initial results in healthy volunteers and patients with chronic pancreatitis. *J Magn Reson Imaging* **20**, 990–997.

[13] El Khouli RH, Macura KJ, Barker PB, Habba MR, Jacobs MA, and Bluemke DA (2009). Relationship of temporal resolution to diagnostic performance for dynamic contrast enhanced MRI of the breast. *J Magn Reson Imaging* **30**, 999–1004.

[14] Hathout E, Chan NK, Tan A, Sakata N, Mace J, Pearce W, Peverini R, Chinnock R, Sowers L, and Obenaus A (2009). In vivo imaging demonstrates a time-line for new vessel formation in islet transplantation. *Pediatr Transplant* **13**, 892–897.

[15] Jain RK (2014). Antiangiogenesis strategies revisited: from starving tumors to alleviating hypoxia. *Cancer Cell* **26**, 605–622.

[16] Kim YR, Savellano MD, Weissleder R, and Bogdanov Jr A (2002). Steady-state and dynamic contrast MR imaging of human prostate cancer xenograft tumors: a comparative study. *Technol Cancer Res Treat* **1**, 489–495.

[17] Marzola P, Degrassi A, Calderan L, Farace P, Crescimanno C, Nicolato E, Giusti A, Pesenti E, Terron A, and Sbarbati A, et al (2004). In vivo assessment of antiangiogenic activity of SU6668 in an experimental colon carcinoma model. *Clin Cancer Res* **10**, 739–750.

[18] Morgan B, Thomas AL, Drevs J, Hennig J, Buchert M, Jivan A, Horsfield MA, Mross K, Ball HA, and Lee L, et al (2003). Dynamic contrast-enhanced magnetic resonance imaging as a biomarker for the pharmacological response of PTK787/ZK 222584, an inhibitor of the vascular endothelial growth factor receptor tyrosine kinases, in patients with advanced colorectal cancer and liver metastases: results from two phase I studies. *J Clin Oncol* **21**, 3955–3964.

[19] Nakamura K, Taguchi E, Miura T, Yamamoto A, Takahashi K, Bichat F, Guilbaud N, Hasegawa K, Kubo K, and Fujiwara Y, et al (2006). KRN951, a highly potent inhibitor of vascular endothelial growth factor receptor tyrosine kinases, has antitumor activities and affects functional vascular properties. *Cancer Res* **66**, 9134–9142.

[20] Ng CS, Raunig DL, Jackson EF, Ashton EA, Kelcz F, Kim KB, Kurzrock R, and McShane TM (2010). Reproducibility of perfusion parameters in dynamic contrast-enhanced MRI of lung and liver tumors: effect on estimates of patient sample size in clinical trials and on individual patient responses. *AJR Am J Roentgenol* **194**, W134–W140.

[21] MY S, Cheung YC, Fruehauf JP, Yu H, Nalcioglu O, Mechetner E, Kyshtoobayeva A, Chen SC, Hsueh S, and McLaren CE, et al (2003). Correlation of dynamic contrast enhancement MRI parameters with microvessel density and VEGF for assessment of angiogenesis in breast cancer. *J Magn Reson Imaging* **18**, 467–477.

[22] Tamada T, Ito K, Sone T, Yamamoto A, Yoshida K, Kakuba K, Tanimoto D, Higashi H, and Yamashita T (2009). Dynamic contrast-enhanced magnetic resonance imaging of abdominal solid organ and major vessel: comparison of enhancement effect between Gd-EOB-DTPA and Gd-DTPA. *J Magn Reson Imaging* **29**, 636–640.

[23] Boxerman JL, Hamberg LM, Rosen BR, and Weisskoff RM (1995). MR contrast due to intravascular magnetic susceptibility perturbations. *Magn Reson Med* **34**, 555–566.

[24] Bremer C, Mustafa M, Bogdanov Jr A, Petrovsky A, and Weissleder R (2003). Steady-state blood volume measurements in Experimental tumors with different angiogenic burdens - a study in mice. *Radiology* **226**, 214–220.

[25] Dennie J, Mandeville J, Boxerman J, Packard S, Rosen B, and Weisskoff RNMR (1998). imaging of changes in vascular morphology due to tumor angiogenesis. *Magn Reson Med* **40**, 793–799.

[26] Guimaraes AR, Rakhlin E, Weissleder R, and Thayer SP (2008). Magnetic resonance imaging monitors physiological changes with antihedgehog therapy in pancreatic adenocarcinoma xenograft model. *Pancreas* **37**, 440–444.

[27] Emblem KE, Farrar CT, Gerstner ER, Batchelor TT, Borra RJ, Rosen BR, Sorensen AG, and Jain RK (2014). Vessel caliber–a potential MRI biomarker of tumour response in clinical trials. *Nat Rev Clin Oncol* **11**, 566–584.

[28] F CT, K WS, L CD, K YR, K SJ, D G, R BR, DT E, J RK, and S AG (2010). In Vivo validation of MRI vessel caliber index measurement methods with intravital optical microscopy in a u87 mouse brain tumor. Neuro. *Oncology* [in press].

[29] Flexman JA, Yung A, Yapp DTT, Ng SSW, and Kozlowski P (2009). Assessment of Vessel Size by MRI in Orthotopic Model of Human Pancreatic Cancer. Annual International IEEE EMBS Conference 2009; Vancouver, BC, Canada. New York, NY: IEEE; 2009. p. 851–854.

[30] Guimaraes AR, Ross R, Figuereido JL, Waterman P, and Weissleder R (2011). MRI with magnetic nanoparticles monitors downstream anti-angiogenic effects of mTOR inhibition. *Mol Imaging Biol* **13**, 314–320.

[31] Jensen JH and Chandra R (2000). MR imaging of microvasculature. *Magn Reson Med* **44**, 224–230.

[32] Kiselev VG, Strecker R, Ziyeh S, Speck O, and Hennig J (2005). Vessel size imaging in humans. *Magn Reson Med* **53**, 553–563.

[33] Lemasson B, Valable S, Farion R, Krainik A, Remy C, and Barbier EL (2013). In vivo imaging of vessel diameter, size, and density: a comparative study between MRI and histology. *Magn Reson Med* **69**, 18–26.

[34] Tropres I, Grimault S, Vaeth A, Grillon E, Julien C, Payen J, Lamalle L, and Decorps M (2001). Vessel size imaging. *Magn Reson Med* **45**, 397–408.

[35] Hingorani SR, Wang L, Multani AS, Combs C, Deramaudt TB, Hruban RH, Rustgi AK, Chang S, and Tuveson DA (2005). Trp53R172H and KrasG12D cooperate to promote chromosomal instability and widely metastatic pancreatic ductal adenocarcinoma in mice. *Cancer Cell* **7**, 469–483.

[36] Fujita M, Hayashi I, Yamashina S, Itoman M, and Majima M (2002). Blockade of angiotensin AT1a receptor signaling reduces tumor growth, angiogenesis, and metastasis. *Biochem Biophys Res Commun* **294**, 441–447.

[37] Otake AH, Mattar AL, Freitas HC, Machado CM, Nonogaki S, Fujihara CK, Zatz R, and Chammas R (2010). Inhibition of angiotensin II receptor 1 limits tumor-associated angiogenesis and attenuates growth of murine melanoma. *Cancer Chemother Pharmacol* **66**, 79–87.